ICMIEE22-170

Comparison of Aerodynamic Performance of NACA 23012 and NACA 4412 Airfoil: A Numerical Approach

Manish Bhadra Arnab[1,*], *Mohammad Ilias Inam*[1]
[1]Department of Mechanical Engineering, Khulna University of Engineering & Technology, Khulna-9203, BANGLADESH

ABSTRACT
Two of the most widely used airfoils worldwide are NACA 23012 and NACA 4412. The purpose of this study is to investigate and compare the aerodynamic characteristics of these two airfoils for a constant Reynolds number of 5×10^6. These simulations were conducted in 2D using Spalart-Allmaras as turbulence model by ANSYS Fluent. Numerical results demonstrate that lift coefficient increases with angle of attack up to certain values, after that it decreases due to flow separation. The drag coefficient also increases with angle of attack for both airfoils. However, the rate of increment is much higher after certain angle of attack due to flow separation. Results also shows that lift coefficient is much higher for NACA 4412 compared to NACA 23012 for each angle of attach. It also observed that critical angle of attack for NACA 23012 is 18˚, whereas flow is separated one degree earlier in NACA 4412. The whole set of simulated results can be considered as a reference to validate computational fluid dynamics analyses of similar studies.

Keywords: CFD, NACA 23012, NACA 4412, Lift-to-drag ratio, Spalart-Allmaras.

1. Introduction

An airfoil is the cross-sectional design of an item, such as a wing, sail, or the blades of a propeller, rotor, or turbine, whose motion through fluid can provide significant lift compared to drag. Lift and drag forces are generated and applied to the airfoil when a fluid flow passes over a body with an airfoil shaped design. The normal force component acting on the airfoil is called lift force and the force component parallel to the motion of the flow is called drag force. Different types of airfoils interact differently with flow passing over it and the generated lift force varies significantly. NACA 23012 and NACA 4412 are two of the most widely used airfoils throughout history. About one tenth of all conventional aircrafts or rotorcrafts have used either of these two airfoils [1]. Three alternative methods, including field testing, analytical/semi-empirical models, and CFD (Computational Fluid Dynamics) can be used in order to study the flow characteristics over such airfoil bodies. The first one, although being quite intricate and expensive, produces exact results. The second one is less reliable, while CFD is the most time and resource efficient method for direct measurements.

Extensive studies have been conducted, both experimentally and analytically on these airfoil shapes. Numerical results vary slightly in comparison with experimental ones due to the nature of governing equations of the turbulence model which is use for the analysis. NASA's Langley Research Center has well documented works on these airfoils [2]. The data provided by Langley Research Center [3] for Re of 1.52 million, which is used to validate the computational method for 13.87^O angle of attack for NACA 4412 airfoil is used to validate the results of this study.

In the case of an aircraft of relatively low speed range and low altitude, Reynolds number around R_e = 5×10^6 can capture the aerodynamic conditions sufficiently. The study is conducted by using Spalart-Allmaras turbulence model.

1.1 Background Study

Two of the most important parameters for this study are lift force and lift coefficient. If the fluid incorporates a circulatory flow around the body, like a spinning cylinder, lift on the body will be generated. The perpendicular component to lift is drag which acts on the parallel direction to the flow. [4]

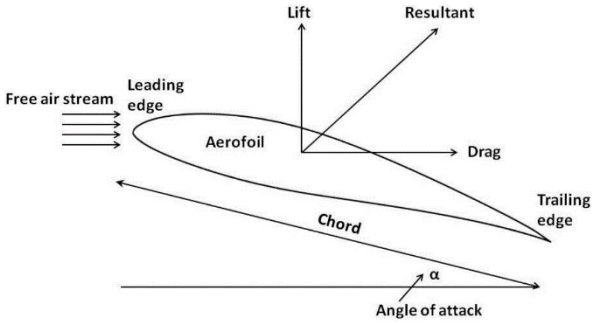

Fig.1 Forces acting on an airfoil [5].

Lift coefficient (C_L) is a dimensionless unit that relates to the lift force to the area and dynamic pressure, where dynamic pressure is determined using fluid mass density and flow speed, shown in Eq (1). For three dimensional wings, the downwash generated near the wing tips reduces the overall C_L of the wing.

$$C_L = \frac{F_L}{0.5\rho V^2 A} \quad (1)$$

Another parameter, drag coefficient (C_D) is another dimensionless quantity that is used to measure the drag

* Corresponding author. Tel.: +88-01725497014
E-mail addresses: m.arnabhadra@gmail.com

or resistance of an object subjected to flow over its body, shown in Eq (2).

$$C_D = \frac{F_D}{0.5\rho V^2 A} \quad (2)$$

Lift-to-drag ratio (L/D ratio) is essentially the ratio between lift coefficient and drag coefficient which is shown in Eq (3). An aircraft with a high L/D ratio indicates that it produces a large amount of lift or a small amount of drag. Large lift means more weight lifting capacity and a small amount of drag means less thrust to drive the aircraft. So, it is critical to measure for the L/D ratio of the airfoils under same conditions.

$$\text{L/D ratio} = \frac{C_L}{C_D} \quad (3)$$

Another important parameter, angle of attack can be defined as the angle between the chord line and streamwise flow direction, shown in Fig. 1. Here the chord length is the distance between the trailing edge and the point where the chord intersects the leading edge. In Fig. 2, the general airfoil design parameters of an airfoil are shown.

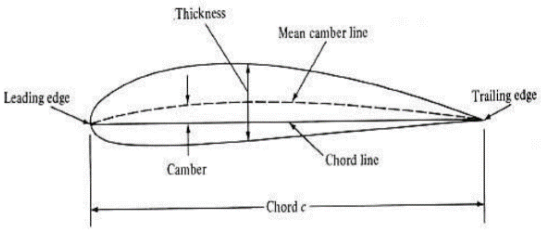

Fig.2 Airfoil design parameters [6].

In flow analysis, the Reynolds number (R_e) is a dimensionless quantity which generally indicates towards the relationship between inertia forces and viscous forces under various fluid flow conditions. The flow separates from an airfoil at the trailing edge. And from those trailing edges, vortices may generate. The flow velocity increases along with the Reynolds number which increases the turbulence as well. So it is considered to compare as the general aerodynamic conditions remain constant under same Reynolds number. Reynolds number can be written as:

$$R_e = \frac{\rho V L}{\mu} \quad (4)$$

2. Methodology

2.1 Airfoil

The following figures, Fig.3 shows NACA 23012 and Fig.4 shows NACA 4412 profile as 2D sketches respectively. The CSV coordinates of the airfoils were taken from NACA airfoil database [7-8], then imported to SOLIDWORKS to create the two-dimensional sketches of the airfoils with 1m chord length for both cases.

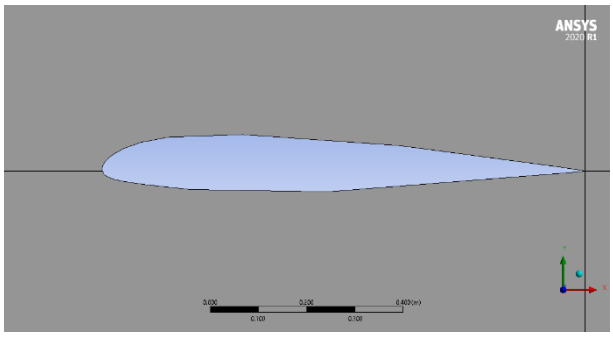

Fig.3 2D NACA 23012 airfoil profile.

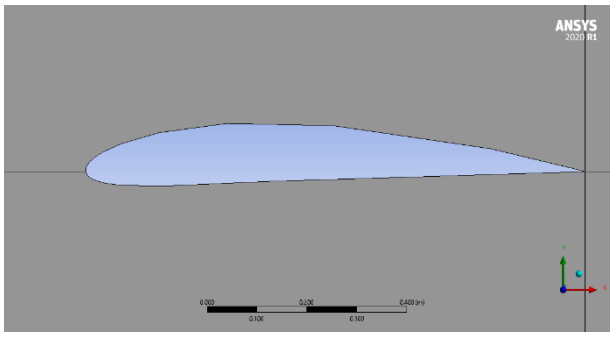

Fig.4 2D NACA 4412 airfoil profile.

2.2 Computational Domain and Mesh Generation

A computational domain, shown in Fig.5 was used for these simulations. Airfoil chord length was assumed one meter. Domain size and different boundary conditions used for this simulation is shown in figures.

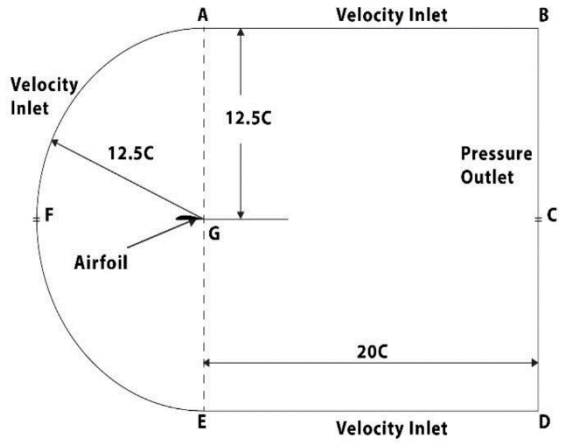

Fig.5 Computation domain [9].

Mesh is important parameter for simulations. For improved convergence and wall function control, C-type mesh was created, shown in Fig. 6. Fine mesh was created near to the wall, shown in Fig. 7.

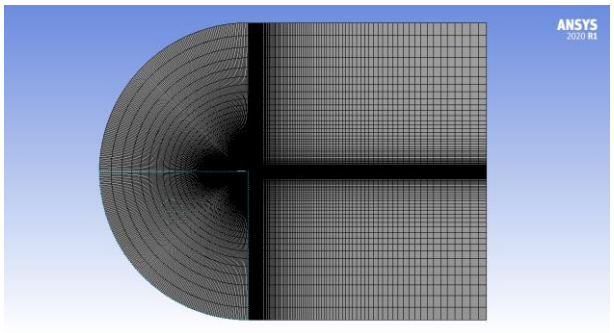

Fig.6 Mesh around the whole domain.

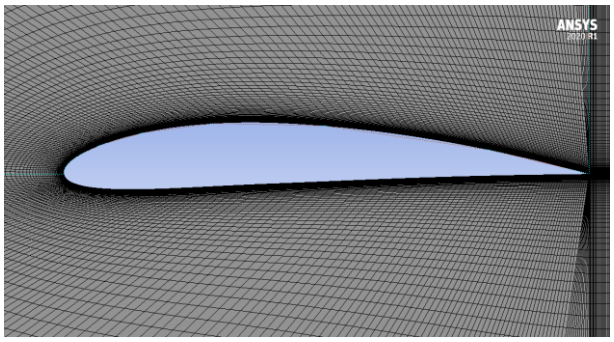

Fig.7 Zoomed in mesh around the airfoil.

While still producing a satisfactory degree of solution, the use of wall functions close to the wall region may significantly improve the overall results. Meshing was adequately biased to create the desired inflation layer. The effective y plus value for solving the turbulence model in viscous sublayer region is $y^+<5$. It is defined as:

$$y^+ = y \times \frac{\sqrt{\frac{\tau\omega}{\rho}}}{\mu} \qquad (5)$$

Here y is defined as the distance from the wall to the centroid of the first fluid cell. For all simulations in this study, y^+ value was always kept bellow 1.

2.3 Mesh Independence Test

Mesh independence test is done in order to determine the most optimized mesh for obtaining a precise numerical result which will also be less resource consuming and time efficient in running the simulations. For this study a set of simulations were conducted by increasing the amount of mesh elements from 15,000 to 144,000 to get the optimized mesh. This was achieved by altering the body edge sizing for each mesh.

NACA 4412 airfoil was considered for this test using Spalart-Allmaras turbulence model. Fig.8 shows the lift to drag ratio for a specific angle of attack of 13.87° in $R_e = 1.52 \times 10^6$.

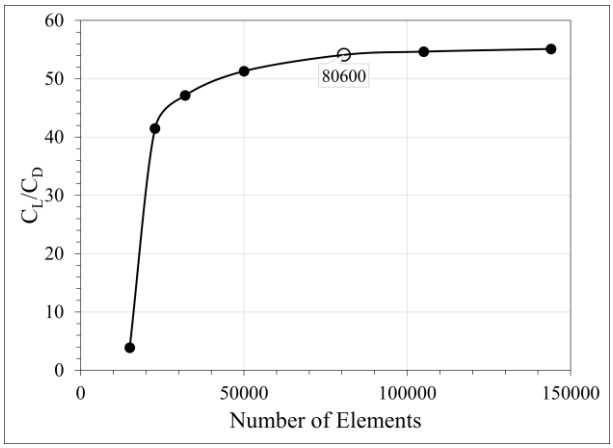

Fig.8 Variation of L/D ratio with number of elements.

It shows that after a certain number of elements are reached, percentage change the lift to drag ratio becomes very insignificant, under 1% which is acceptable and thus the mesh with 80,600 elements is considered as ideal and is used for all the numerical simulations of both airfoil profiles.

2.4 Numerical Conditions

To compute and validate the solver scheme, both airfoils were generated with 1m in chord length with a far field having 81164 nodes and 80600 elements. Biased edge sizing was used in mesh to maintain a reasonable y+. Outlet condition was kept as pressure outlet type. Hybrid initialization with external aero-favorable settings was used for computation.

Table 1 Boundary conditions

No	Input	Value
1	Type of fluid	Air
2	Fluid density	1.225 [kg/m^3]
3	Flow velocity	73.037 [m/s]
4	Operating pressure	101325 Pa
5	Operating temperature	288.16 K
6	Reynolds Number	5×10^6
7	Chord length	1 M
8	Model	Spalart-Allmaras
9	Viscosity	1.7894×10^5 [kg/ms]

2.5 Turbulence Model

With only one equation, the Spalart-Allmaras turbulence model is primarily intended for straightforward external aerodynamic analysis. A transport equation for eddy viscosity is included in this model. Here the distribution of the Reynolds stress is determined in order to create a closed system of the central equation for the mean motion of a flow. In this analysis, strain/vorticity-based SA model is used with a turbulent viscosity ratio of 1.

The working variable $\hat{v}$ transport equation is given by,

$$\frac{\partial \hat{v}}{\partial t} + u_j \frac{\partial \hat{v}}{\partial x_j} = c_{b1}(1 - f_{t2})\hat{S}\hat{v} - \left[c_{w1} f_w - \frac{c_{b1}}{k^2} f_{t2}\right]\left(\frac{\hat{v}}{d}\right)^2 + \frac{1}{\sigma}\left[\frac{\partial}{\partial x_j}\left((v + \hat{v})\frac{\partial \hat{v}}{\partial x_j}\right) + c_{b2}\frac{\partial \hat{v}}{\partial x_i}\frac{\partial \hat{v}}{\partial x_i}\right] \quad (6)$$

and the turbulent eddy viscosity is computed from:

$$\mu_t = \rho \hat{v} f_{v1} \quad (7)$$

here,

$$f_{v1} = \frac{\chi^3}{\chi^3 + c_{v1}^3} \quad (8)$$

$$\chi = \frac{\hat{v}}{v} \quad (9)$$

and ρ is the density, $v = \frac{\mu}{\rho}$ is the molecular kinematic viscosity, and μ is the molecular dynamic viscosity. Additional definitions are given by the following equations:

$$\hat{S} = \Omega + \frac{\hat{v}}{k^2 d^2} f_{v2} \quad (10)$$

Here $\Omega = \sqrt{2W_{ij}W_{ij}}$ is the magnitude of the vorticity, *d* is the distance from the field point to the nearest wall, and

$$f_{v2} = 1 - \frac{\chi}{1 + \chi f_{v1}} \qquad f_w = g\left[\frac{1 + c_{w3}^6}{g^6 + c_{w3}^6}\right]$$

$$g = r + c_{w2}(r^6 - r) \qquad r = \min\left[\frac{\hat{v}}{\hat{S}k^2 d^2}, 10\right]$$

$$f_{t2} = c_{t3}(-c_{t4}\chi^2) \qquad W_{ij} = \frac{1}{2}\left(\frac{\partial u_i}{\partial x_j} - \frac{\partial u_j}{\partial x_i}\right)$$

The boundary conditions are:

$$\hat{v}_{wall} = 0$$

$$\hat{v}_{farfield} = 3v_\infty : to : 5v_\infty$$

These boundary conditions on the SA turbulence field variable correspond to turbulent kinematic viscosity values of:

$$v_{t,wall} = 0$$

$$v_{tfarfield} = 0.210438v_\infty : to : 1.294234v_\infty$$

The constants are:

$$c_{b1} = 0.1355 \qquad \sigma = \frac{2}{3} \qquad c_{b2} = 0.622 \qquad k = 0.41'$$

$$c_{w2} = 0.3 \qquad c_{w3} = 2 \qquad c_{v1} = 7.1$$

$$c_{t3} = 1.2 \qquad c_{t4} = 0.5 \qquad c_{w1} = \frac{c_{b1}}{k^2} + \frac{1 + c_{b2}}{\sigma}$$

The Spalart-Allmaras model has production and destruction source terms that are non-zero in the freestream conditions, even when vorticity is zero. The source terms are, however, very small: proportional to $1/d^2$ [9].

2.6 Validation of the process

Data provided by Langley Research Center [3] is used to validate the simulation method. The method primarily ran the computations for NACA 4412 with 13.87^O angle of attack. Then the C_P data is compared by overlapping on the curve generated by the Langley Research Center pressure data. Fig. 9 shows the comparison. Here the plot shows comparison with the Spalart-Allmaras results from an independent CFD code, CFL3D by NASA.

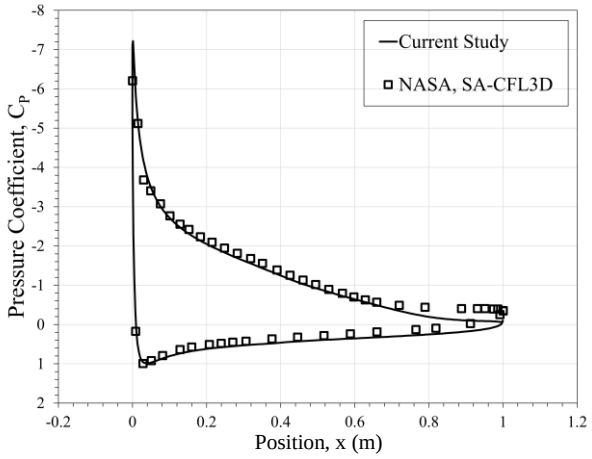

Fig.9 Pressure coefficient on the airfoil surface at 13.87° angle of attack.

3. Result and Discussion

3.1 Lift and drag coefficients

The following Fig.10 shows lift coefficient plotted against different values of α for NACA 23012 and NACA 4412 airfoil profiles. Similarly, Fig.11 shows the variation of drag coefficient and Fig.12 shows the variation of L/D ratio for both airfoils computed under same Reynolds number and boundary conditions.

The critical angle of attack or the stall angle of attack where maximum lift occurs is determined to be:

Table 2 Critical angle of attack at $R_e = 5\times10^6$

Airfoil	Critical Angle of Attack
NACA 23012	18°
NACA 4412	17°

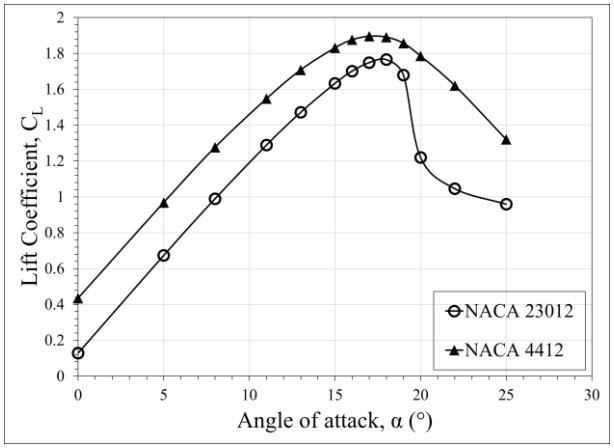

Fig.10 Variation of C_L for different angles of attack of NACA 23012 and NACA 4412

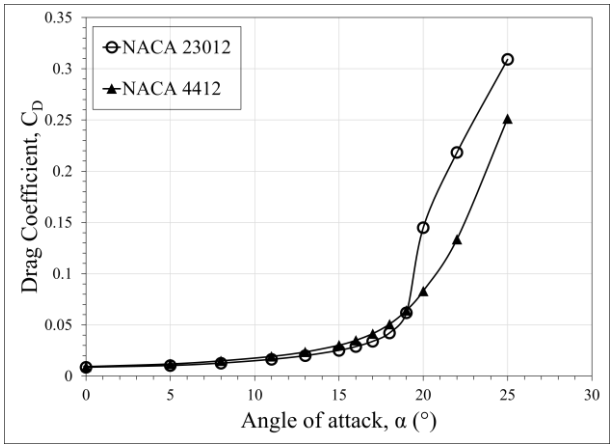

Fig.11 Variation of C_D for different angles of attack of NACA 23012 and NACA 4412

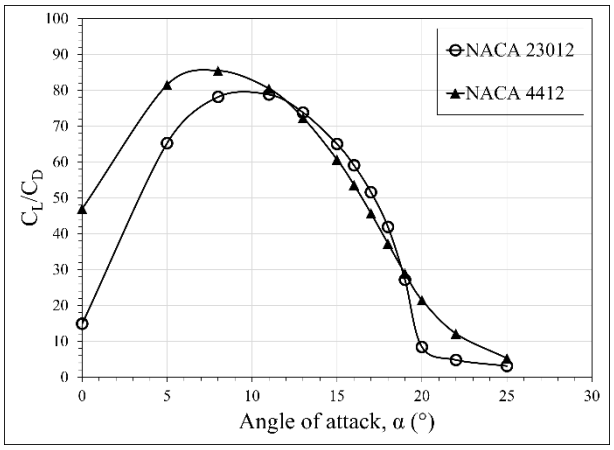

Fig.12 Variation of L/D ratio for different angles of attack of NACA 23012 and NACA 4412

The drastic differences in lift and drag coefficients between the two airfoils after flow separation occurs, shown in fig.10 and fig.11, is due the notable difference is geometry, specially at the rear end of the two airfoils. Also, from Fig.12, for higher angles of attack, after 11°, both airfoils perform similarly but for lower angles of attack, NACA 4412 airfoil performs significantly better.

3.2 Static Pressure Contour

From fig.13, it can be observed that as angle of attack increases, pressure difference between top and bottom surface also increases for both airfoils.

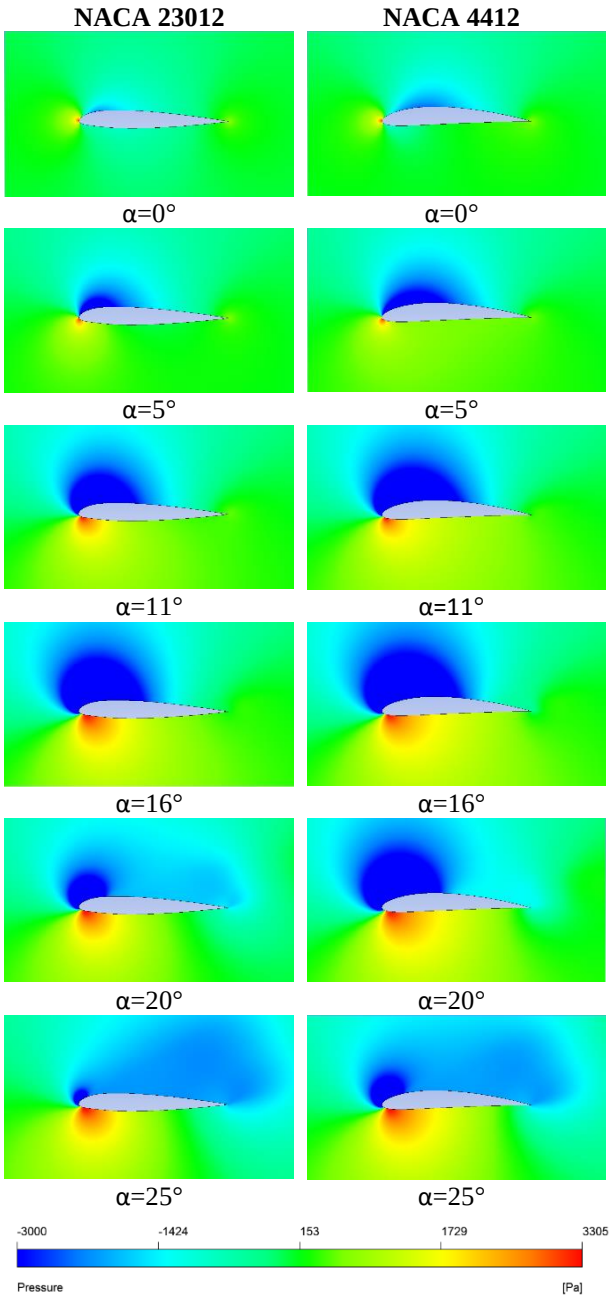

Fig.13 Static Pressure Contours at different angles of attack of NACA 23012 and NACA 4412.

3.3 Velocity Contour

Velocity contours of the two airfoils, NACA 23012 and NACA 4412 for different angles of attack can be seen by in Fig.14 below. It is observed that as angle of attack increases, trailing edge separation occurs earlier for both.

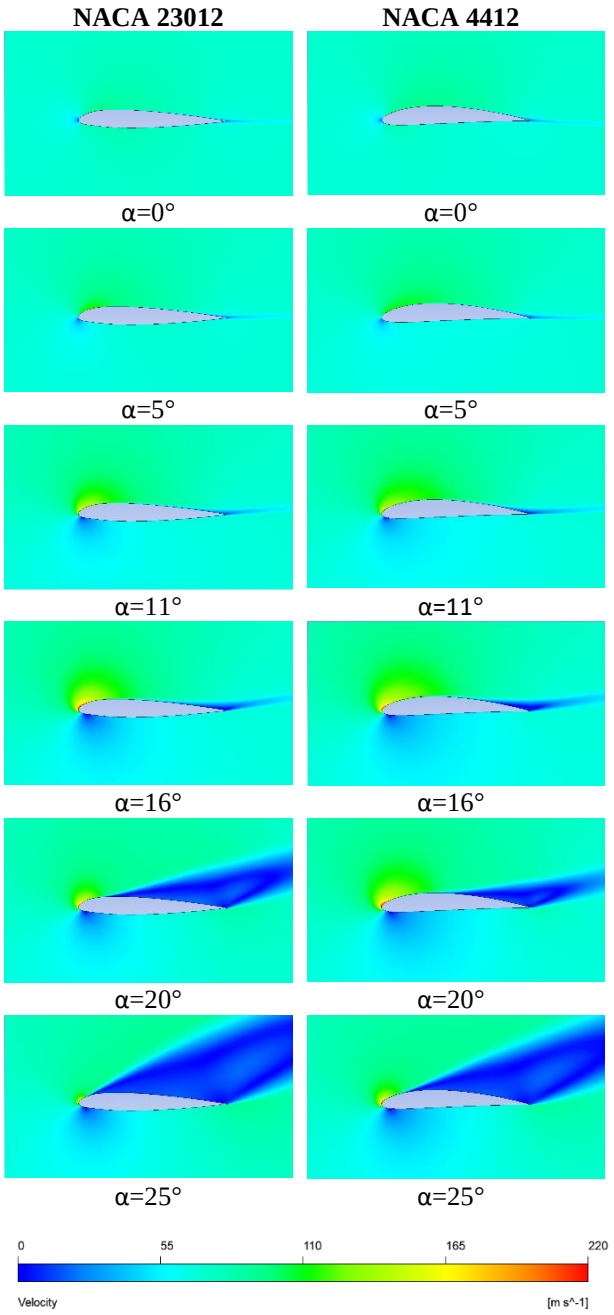

Fig.14 Velocity Contours at different angles of attack of NACA 23012 and NACA 4412.

3.4 Variation of Pressure Coefficient

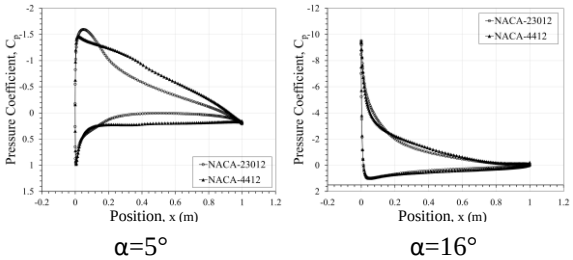

α=5° α=16°

Fig. 15 Variation of C_P along the surfaces of NACA 23012 and NACA 4412 airfoil.

4. Conclusion

In this study, the aerodynamic behaviors of NACA 23012 and NACA 4412 profiles were observed and compared using Spalart-Allmaras turbulence model at $R_e = 5\times10^6$. It is observed that NACA 4412 airfoil generates more lift force than NACA 23012 airfoil. But for higher angles of attack, both airfoils demonstrate almost similar performance. Also, the trailing edge flow separation occurs a degree later for NACA 23012 airfoil.

5. References

[1] https://m-selig.ae.illinois.edu/ads/aircraft.html (Accessed: 13-Nov-2022).
[2] https://turbmodels.larc.nasa.gov/naca4412sep_val.html (Accessed: 13-Nov-2022).
[3] https://turbmodels.larc.nasa.gov/naca4412sep_val_sa.html (Accessed: 13-Nov-2022).
[4] Burton, T., Jenkins, N, Sharpe, D. and Bossanyi, E. Wind Energy Handbook. Chichester, UK: John Wiley & Sons, 2011; 65-67
[5] Panigrahi, D.C., Mishra D.P., CFD Simulations for the Selection of an Appropriate Blade Profile for Improving Energy Efficiency in Axial Flow Mine Ventilation Fans, Journal of Sustainable Mining, 2014; Volume 13, Issue 1, Pages 15-21, ISSN 2300-3960.
[6] Yılmaz M., Koten H., Çetinkaya, E, Coşar, Z., A comparative CFD analysis of NACA0012 and NACA4412 airfoils. Journal of Energy Systems 2018; 2(4): 145- 159, DOI: 10.30521/jes.454193.
[7] http://airfoiltools.com/airfoil/details?airfoil=naca4412-il (Accessed: 13-Nov-2022).
[8] http://airfoiltools.com/airfoil/details?airfoil=naca23012-il (Accessed: 13-Nov-2022).
[9] Pranto, M.R.I. and Inam, M.I., 2020. Numerical Analysis of the Aerodynamic Characteristics of NACA4312 Airfoil. Journal of Engineering Advancements, 1(02), pp.29-36.
[10] Spalart, P.R., Allmaras S.R., A one-equation turbulence model for aerodynamic flows, AIAA 30th aerospace sciences meeting and exibit, 6-9 Jan 1993.

NOMENCLATURE

V : velocity, m/s
ρ : density, Kg/m^3
υ : kinematic viscosity, m^2-s
μ : dynamic viscosity, Pa-s
C_p : coefficient of pressure
C_L : coefficient of lift
C_D : coefficient of drag
R_e : Reynolds number
c/L : chord length, m
α : angle of attack, degree
x : x axial position in the airfoil, m
i,j,k : cartesian unit vector